Thermal Flux Probe for Characterization of the Ion Source: Background Pressure Effects

Stanislav Musikhin[1], Ivan Romadanov[2], and Yevgeny Raitses[3]
Princeton Plasma Physics Laboratory, Princeton, NJ 08540, USA

This work presents the development and deployment of a thermal flux probe (calorimetric probe) for characterization of the plasma plume of a gridded ion source under varying background pressures. The background pressure can significantly alter plume characteristics including velocity distribution functions for ions and atoms/molecules, and plume angle for ion thrusters and Hall thrusters. The charge exchange (CEX) collisions between accelerated ions and slow background gas atoms/molecules results in the formation of a fast neutral flow and slow ion population. The latter also contributes to plume broadening. In this paper, we study the CEX process for the plume of the gridded ion source in the pressure range of 10^{-5} torr to 10^{-3} Torr. This background pressure range is relevant to environments at the thruster test facilities and industrial applications of these plasma sources. We also discuss the encountered challenges for reliable measurements of the fast neutral beam, such as thermal flux probe calibration and creation of slow ions due to the charge-exchange process.

I. Nomenclature

CEX	=	charge exchange
C_c	=	effective heat capacity of the collector
H_c	=	enthalpy of the collector
P_{total}	=	total incoming power experienced by the collector
$P_{\text{fast ions}}$	=	power delivered by fast ions
$P_{\text{fast neutrals}}$	=	power delivered by fast neutrals
P_{rad}	=	power delivered by radiation
$P_{\text{slow ions}}$	=	power delivered by slow ions
$P_{\text{electrons}}$	=	power delivered by electrons
P_{recomb}	=	power delivered by recombination
T_c	=	temperature of the collector

II. Introduction

The characterization of electric propulsion thrusters is crucial for their performance validation and fundamental understanding of plasma plume behavior. The latter is significantly influenced by the charge-exchange (CEX) process, where energetic ions collide with slow background neutrals, resulting in the formation of energetic neutrals and slow ions. Here, we investigate the effect of the ambient environment, specifically looking into how the background gas pressure in the vacuum chamber can alter the CEX process. For that, we designed and deployed a thermal flux probe directly into the ion beam generated by the ion source.

The thermal flux probe, also called the calorimetric probe or passive thermal probe [1], [2], [3], is a diagnostic tool capable of quantifying the total and individual heat fluxes transferred from a plasma to a surface. The concept of the

[1] Associate Research Physicist
[2] Staff Research Physicist
[3] Principal Research Physicist, AIAA Associate Fellow

thermal flux probe was introduced by Thornton to measure energy fluxes to a substrate in plasma processing applications [2]. The principle involves measuring the temporal temperature change of a thermally isolated "substrate dummy" that is exposed to various energy fluxes. Crucially, by electrically biasing the probe, the contributions can be differentiated, e.g., heating by fast ions, fast neutrals, electrons, recombination, etc. Furthermore, when thermal flux (caused by fast ions and fast neutrals) is measured simultaneously with the current through the probe (caused by a flux of ions), the charge-exchange ratio can be calculated [1].

III. Experimental

The experiments were conducted inside a stainless-steel vacuum vessel about 1 m in length and 0.8 m in diameter (Small Hall Thruster facility at Princeton Plasma Physics Laboratory) [4]. The vacuum chamber was grounded and served as a reference for all electrical measurements. Vacuum conditions were achieved using a blower, a mechanical pump, and an Osaka TG3203M turbo-molecular pump, providing a base pressure of about $3 \cdot 10^{-6}$ Torr. Pressure was monitored by an external ion gauge (Kurt Lesker, KJLC 392), and corrected for the gas type.

Two mass flow controllers (Alicat) supplied argon gas to the chamber. One fed the gas to the ion source, while another provided the additional argon flow directly to the vacuum chamber to vary the background gas pressure.

A 3-cm diameter Kaufman-type gridded ion source was used. The source had two tungsten filaments: one (the cathode filament) maintained the discharge, and the other (the neutralizer filament) was placed outside the source to neutralize the extracted ion beam. Plasma was generated inside the anode chamber of the source, which was positively biased with respect to the tungsten filament cathode. For the ion beam extraction, the anode chamber of the source was positively biased with respect to the acceleration grid. Typical conditions used in the experiments were: the argon gas flow rate to the ion source of 4.6 sccm, the gas flow rate to the chamber of 0—186 scmm, the anode discharge voltage of 40 V, the accelerating voltage of 400 eV. The cathode and neutralizer filaments were heated at 8 A and 7.5 A, respectively. The pressure inside the chamber was stable between 0.03—1.14 mTorr, for gas flows 0—186 scmm, which corresponds to the achieved pumping speeds of 2000±150 l/s for argon. A warm-up period of 45 minutes was observed to allow the beam current to stabilize before measurements.

A. Thermal Flux Probe: Design and Working Principle

To measure the ratio of fast ions to fast neutrals created due to the charge-exchange, we have assembled, calibrated, and deployed a thermal flux probe. Figure 1a shows a photograph of the assembled probe. The body of the probe was made of ceramic (Macor) for thermal and electrical insulation, while the sensitive substrate is made of a thin tantalum foil (~50 μm thick, 20 mm diameter). A large mass of the ceramic body and its high specific heat capacity ensured small temperature variation during an experiment. Tantalum was chosen due to its low sputtering yield and small secondary electron emission [5], [6], while the substrate's small mass enhances its thermal sensitivity. A tantalum foil band was attached to the side as an additional probe to monitor slow ions (Figure 1b).

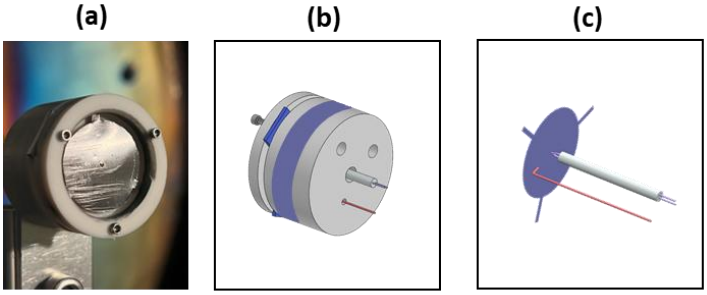

Fig. 1 (a) Photograph of the assembled thermal flux probe, front side; (b) Sketch of the assembled thermal flux probe, sideview, showing the side probe and wire with thermocouple connections; (c) Sketch of the plasma-facing collector (blue) showing the spot-welded thermocouple and wire. The collector was made of a thin tantalum foil, while the probe body was made of Macor. The foil had minimal thermal contact with the probe body through three extensions seen in (c).

Figure 2 shows the experimental assembly inside the vacuum chamber. The thermal flux probe position was varied with respect to the ion source.

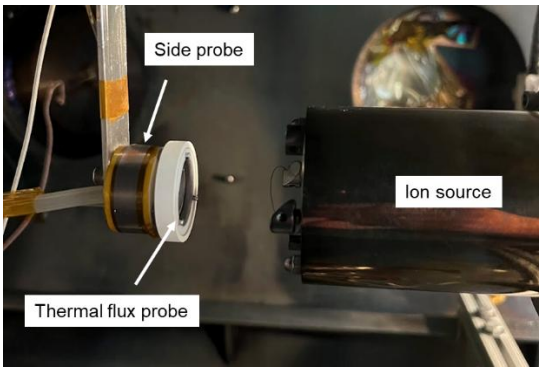

Fig. 2 Experimental setup showing the ion source and the thermal flux probe with the side foil to measure slow ions contribution.

A thermocouple was spot-welded to the back side of the tantalum substrate (Figure 1c) to measure its temperature in real time. The thermocouple wires were connected to a readout unit through a feedthrough. The output voltage was then logged in real time by an NI DAQ system through a LabView interface. The temperature logging part of the probe was upgraded between the two experimental campaigns, an initial type C thermocouple and Omega DP20-M1 readout unit were swapped for a type K thermocouple and Dataforth DSCA47K-05 readout unit. That upgrade improved the temperature measurement accuracy and the readout speed. In addition to the thermocouple, a wire was spot-welded to the back side of the tantalum substrate (Figure 1c), which was used: (i) to measure ion current flowing through the substrate; and (ii) to bias the substrate. Both the thermocouple and the bias wires were electrically insulated to avoid electrical interferences.

The change of the thermal probe enthalpy is given by

$$\frac{dH_c}{dt} = C_{\mathrm{c}} \frac{dT_{\mathrm{c}}}{dt}\,, \tag{1}$$

where C_{c} is the effective heat capacity of the collector, which we find by the probe calibration described below, and $\frac{dT_{\mathrm{c}}}{dt}$ is the change in the probe temperature, which is measured experimentally. During the collector heating by an ion beam, the energy balance is described by

$$\frac{dH_{\mathrm{c,heating}}}{dt} = P_{\mathrm{in}} - P_{\mathrm{out}}(T_{\mathrm{c}})\,, \tag{2}$$

and during the collector cooling (no ion beam) by

$$\frac{dH_{\mathrm{c,cooling}}}{dt} = -P_{\mathrm{out}}(T_{\mathrm{c}})\,, \tag{3}$$

If the incoming power P_{in} is constant during heating, which is a reasonable assumption for short heating duration under 30 s and stable ion source operation, and assuming heat losses are defined only by the probe temperature, Eq. 3 can be subtracted from Eq. 2 to yield the incoming power

$$P_{\mathrm{in}}(T_{\mathrm{c}}) = C_{\mathrm{c}} \left(\frac{dT_{\mathrm{c,heating}}}{dt} - \frac{dT_{\mathrm{c,cooling}}}{dt} \right)_{T_{\mathrm{c}}} = C_{\mathrm{c}} \cdot F(T_{\mathrm{c}}), \tag{4}$$

where $F(T_{\mathrm{c}})$ is the difference of the temperature derivatives.

Total incoming power experienced by the collector, P_{total}, is given by

$$P_{\mathrm{total}} = P_{\mathrm{fast\,ions}} + P_{\mathrm{fast\,neutrals}} + P_{\mathrm{rad}} + P_{\mathrm{slow\,ions}} + P_{\mathrm{electrons}} + P_{\mathrm{recomb}}. \tag{5}$$

It includes energy influx from fast ions and fast neutrals, heat radiation from hot filaments, energy influx from slow ions that are created due to charge-exchange process, energy influx from electrons, and energy influx due to recombination of ions and electrons at the collector surface. Heat radiation from hot filaments is constant during both heating and cooling, and hence, cancels out during differentiating. The collector is biased negatively so that electrons are effectively repelled. Therefore, the power measured during an experiment and calculated using Eq. 4 is given by

$$P_{\text{in}} = P_{\text{fast ions}} + P_{\text{fast neutrals}} + P_{\text{slow ions}} + P_{\text{recomb}}. \tag{6}$$

With electrons being repelled, only ions bring charge and contribute to the current measured at the substrate, $I_c = I_{\text{fast ions}} + I_{\text{slow ions}}$. Therefore, the ion power contribution can be calculated as

$$P_{\text{ions}} = P_{\text{fast ions}} + P_{\text{slow ions}} = I_{\text{fast ions}}(U_{\text{beam}} + U_c) + I_{\text{slow ions}}(U_c), \tag{7}$$

where U_{beam} is the ion beam energy set by the anode voltage (typically, 400 V), and U_c is the negative collector bias to repel electrons (20 V). The effect of slow ions, i.e., their current contribution, $I_{\text{slow ions}}$, was measured using the side probe shown in Figure 1b, additionally accounting for the fact that the side and front collectors have different areas. The power due to recombination of ions at the surface is given by $P_{\text{recomb}} = I_c(E_{\text{ion}} - E_W)$, where E_{ion} = 15.8 eV is the ionization energy of argon, and E_W = 4.3 eV is the electron work function of tantalum.

Furthermore, fast ions hitting the substrate could lead to production of secondary electrons, which would lead to measured currents being higher than the actual ion current. However, the substrate material was specifically chosen to minimize production of secondary electrons, leading to an estimated error up to 2—3% of the ion current [7]. Therefore, the contribution of secondary electrons from the collector surface was neglected here.

Additionally, metastable argon atoms could quench on the probe surface releasing up to 11.7 eV per quenching event [8], contributing to the thermal flux. However, given that the metastable fraction is expected to be orders of magnitude lower than the ground-state population [9] and their potential energy is significantly lower than the kinetic energy of the accelerated species (~400 eV), the thermal contribution of metastable quenching was assumed to be negligible.

Finally, the charge-exchange can be calculated by

$$\text{CEX}\ (\%) = 100 \cdot \frac{P_{\text{fast neutrals}}}{P_{\text{fast ions}} + P_{\text{fast neutrals}}}, \tag{8}$$

where $P_{\text{fast neutrals}} = P_{\text{in}} - P_{\text{fast ions}} - P_{\text{slow ions}} - P_{\text{recomb}}$.

Figure 3a shows a typical temperature trace of the thermal flux probe during heating by the ion beam and cooling when the ion beam is turned off. Raw temperatures are fit using exponential curves. The fitted curves are then differentiated ($F(T_s)$, Figure 3b), and the difference of two derivatives, is shown in Figure 3c. The mean value $\langle F(T_s)\rangle$ is plugged into the Eq. 4 to find $\langle P_{\text{in}}(T_s)\rangle$, while the spread of $F(T_s)$ is taken as the error bar.

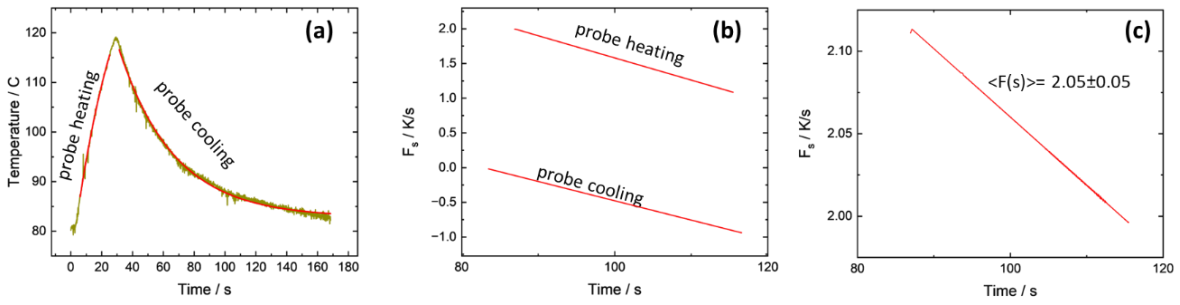

Fig. 3 (a) Typical temperature trace of the thermal flux probe during an experiment; (b) Temperature derivatives; (c) The difference of two derivatives, $F(T_s)$.

B. Thermal Flux Probe: Calibration

Eq. 4 includes the effective heat capacity of the thermal flux probe's substrate, which accounts for contributions from the substrate material, welding dots, thermocouple junction, and connected bias wire, and hence, must be measured experimentally. These measurements were performed in the same vacuum chamber as the charge-exchange experiments but using only electrons as the heating source. Hence, no plasma was ignited, instead a neutralizer filament was heated to produce electrons. The probe's substrate was positively biased (U_s = +800..+1500 V) to accelerate the incident electrons. The calibration experiments were taken in a space-charge-limited regime (electron current following the Child-Langmuir law). In future work, we will extend the calibration to a filament-temperature-limited regime (electron current following the Richardson-Dushman law) to reduce potential space-charge shielding effects.

The thermal flux probe was positioned at different distances from the filament, e.g., 10, 15, and 20 cm, to imitate the charge exchange measurements. The chamber pressure was 4×10^{-6} Torr to minimize electron scattering. The resulting electron power is given by

$$P_e = P_{in} = I_s\left(U_s + \frac{U_{fil}}{2}\right), \tag{9}$$

where $\frac{U_{fil}}{2}\sim 5$ V accounts for the mean voltage drop along the filament. The substrate is also heated by radiation from the hot filament, however, that radiation is constant during both heating and cooling and hence cancels out during differentiation. Therefore, the effective heat capacity, $\langle C_s\rangle$, can be find from Eq. 4 as

$$\langle C_s\rangle = \frac{\langle F(T_s)\rangle}{P_e}. \tag{10}$$

Figure 4 shows the measured electron power, P_e, versus $\langle F(T_s)\rangle$ measured at different distances between the thermal flux probe and the electron source, L. The $\langle C_s\rangle$ was found as a slope of the linear fit to the data. Root-MSE (Root Mean Square Error) is a goodness-of-fit parameter that measures the quality of a linear fit, particularly when forcing the intercept through zero (as here), where R^2 parameter is unreliable. The probe was mounted on a rod using a Wilson seal, allowing for manual adjustment to the required position. The movement involved no mechanical changes to the probe itself; thus, the heat capacity was expected to remain constant regardless of distance between the probe and the emitting source. Yet, the obtained effective heat capacities were found to increase with distance, from 164 J/K at 10 cm to 310 mJ/K at 20 cm

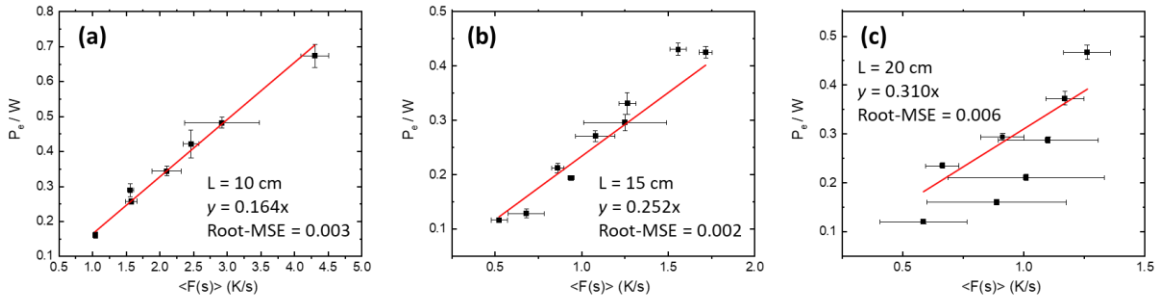

Fig. 4 Electron power, P_e, versus $\langle F(T_c)\rangle$ calculated from the collector temperature curves. The effective heat capacity found as the slope of the linear fit to the data with the intercept fixed at zero. Measurements were performed at different distances from the electron source.

While not fully understood yet, several mechanisms may contribute to the observed discrepancies.

1) It may be due to electron-induced secondary electron emission (SEE) from the ceramic holder surrounding the collector. The secondary electrons emitted from the surface could contribute to the collected current, resulting in an overestimation of the measured power, particularly at distances closer to the emitting source. The SEE yields for insulating ceramics, such as Macor, are expected to be > 1 at relevant electron energies here (800—1500 eV) [10].

2) Dielectric charging may result in current leakage to the probe, which was detected and resolved in Ref. [11] by covering the dielectric part with a grounded metal foil.

3) Distance-dependent variation in SEE from the chamber walls could be an issue.

4) At closer distances to the emitting filament, the fringing fields increase the curvature of electron trajectories, leading to oblique angles of incidence. This may result in the increasing electrons backscattering and hence increased energy deposition.

Here, we addressed some but not all of the described scenarios.

Scenarios 1 and 2, dielectric charging and secondary electron emission from the ceramic holder, could be simultaneously mitigated if shielding the ceramic part with a conductive material. Here, we covered the Macor body with a grounded tantalum foil. Nevertheless, the calibration measurements continued to show heat capacity values increasing with distance from the electron source.

To eliminate the possible influence of the chamber walls, as described in scenario 3, the volume between the thermal probe and the filament was enclosed within a stainless-steel cylindrical shield. This ensured that electron trajectories were geometrically isolated from the chamber vessel. The shield was biased to +8 V while the emitting filament potential was approximately +7 V, both relative to ground. When the sheet was grounded or floating, no current was detected at the thermal probe collector surface, suggesting that the electrons were repelled. This calibration was performed following the partial upgrade of the thermal flux probe described above. Although the collector and the ceramic parts remained unchanged, the spot-welding on the back side was redone to incorporate a different thermocouple. Hence, it was expected that the effective heat capacity could differ from the one found in the previous calibration. Figure 5 shows the resulting heat capacity versus distance. Here, the effective heat capacity value was constant between 5—15 cm (~170 mJ/K, similar to the previous calibration) and decreasing beyond that. The decreasing trend with distance is opposite what was observed in the first calibration dataset.

Ultimately, the mechanism causing the heat capacity of the probe to vary with its distance from the filament remains undetermined. The ongoing efforts are focused on mitigating the remaining calibration challenges. Subsequent analysis was done using a constant value of $\langle C_s \rangle = 165$ mJ/K, which was consistent across both calibration sets, even after re-welding of the wires.

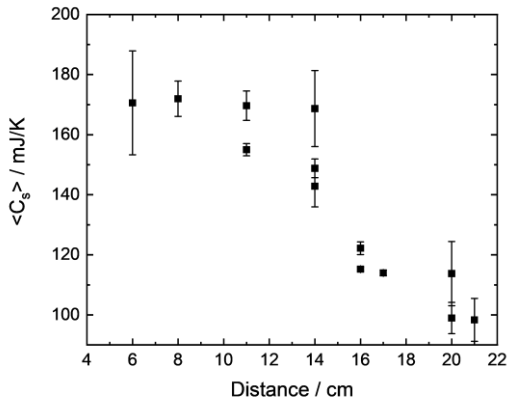

Fig. 5 Effective heat capacity, $\langle C_s \rangle$ versus distance between the thermal flux probe and the emitting filament. Thermal probe was inserted inside a positively biased stainless-steel cylinder to eliminate the influence of chamber walls on calibration.

IV. Results and Discussion

Figure 6 shows measured charge-exchange ratios in % versus background gas pressure. E.g., CEX = 70 % implies that 70 % of the fast ions underwent charge-exchange process and were converted into fast neutrals. Two experimental runs correspond to the measurements that deployed the thermal flux probe before (Run 1) and after (Run 2) the slight upgrade. The argon pressure in the chamber was varied between 0.03—1.14 mTorr, while the distance between the thermal flux probe and the ion source was kept at 20 cm. Higher gas pressures could not be used as it led to arcing between the ion source grids. For theoretical CEX predictions, we used the energy-dependent cross-section for resonant Ar charge-exchange collisions from Refs. [12], [13]: $\sigma_{CEX} = 5.75 \cdot 10^{-15} \cdot U_{beam}^{-0.1}$ [cm^2], where U_{beam} is the beam energy in eV. The mean free path then is given by $\lambda_{CEX} = 1/(\sigma_{CEX} \cdot n_{Ar})$, where n_{Ar} is the argon concentration

found from the ideal gas law. Following these expressions, pressures between 0.03—1.14 mTorr correspond to the λ_{CEX} between 9—330 cm. The shaded area represents ±15% uncertainty in the measured pressure, typical to the ion gauge.

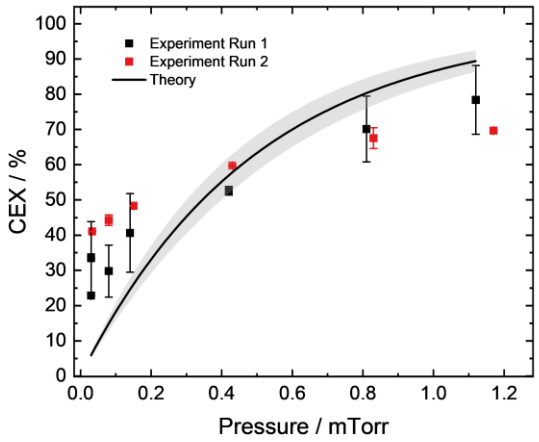

Fig. 6 Charge-exchange (CEX) ratios versus background argon pressure for 20 cm pathway. Shaded area represents ±15% pressure measurements uncertainty.

The CEX ratio expectedly increases with the distance from the ion source. We must remind though about the unresolved issues with the calibration, which warrant caution to any quantitative analysis. Nevertheless, it can be stated that experimental CEX values are anomalously high at low pressures, where no CEX collisions are expected. We associate that with the CEX processes occurring inside the ion source and in its immediate vicinity, where background pressure can be much higher than in the rest of the vacuum chamber [14]. To correct for this offset, we measured CEX values versus distance (Figure 7) and normalized the results to the closest measurement position (here, 5 cm from the ion source), using that point as the effective starting point (i.e., as 0 cm) for both experiment and theory.

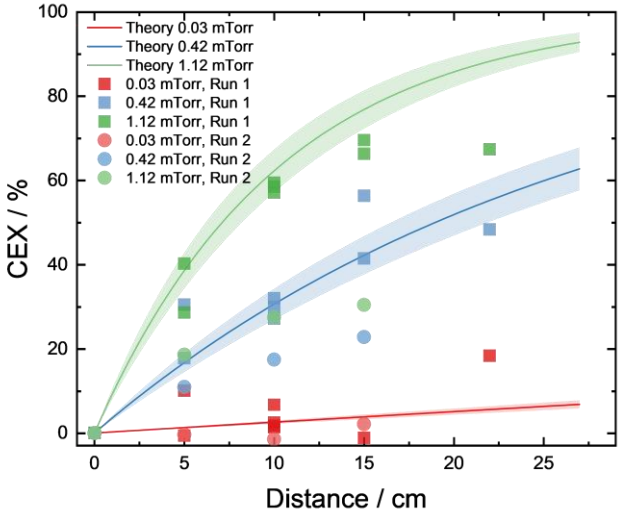

Fig. 7 Charge-exchange (CEX) ratios versus distance from the ion source. Squares and circles correspond to experimental values as measured with a thermal flux probe; solid curves correspond to theoretical

predictions. Shaded areas represent ±15% pressure measurements uncertainty. All data were normalized to the measurement position closest to the ion source.

As seen in Figure 7, the general trend is that the charge-exchange effect accumulates with distance, as expected from the theory. Also, after normalization to the closest measurement position, the CEX effect is expectedly negligible at the lowest pressure. The mismatch between the two experimental runs is being investigated through supplementary experiments. Notably, at larger distances (>15 cm) and higher pressures (e.g., 1.12 mTorr), the experimental data not only deviates from the theoretical model suggesting CEX values significantly smaller than the prediction, but it also "plateaus". Apart from the obvious problem with the thermal probe calibration, we attribute this to factors associated with the background pressure effects. For example, our measurements suggested that the ion beam diverges with pressure and distance, as described in the next paragraph. This could affect the experimental CEX values at higher pressures and longer distances. The discrepancy is further compounded by the unaccounted scattering process, which amplifies with pressure and, furthermore, differs for ions and neutrals.

We characterized the plume angle using a flat electrostatic probe with a guarding sleeve, installed on a high precision rotating system with a vacuum compatible stepper motor. Additional details can be found elsewhere [15]. Both flat probe and guarding sleeve were biased to –30 V to ensure ion current saturation. Measurements were taken while the probe rotated between ±90° relative to the ion source axis. To account for the contribution of the background plasma, the ion current measured at the 90° position relative to the thruster axis was subtracted from measurements taken at other angular positions. Data acquisition was performed utilizing 10:1 voltage dividers and logged by an NI DAQ system through a LabView interface. Figure 8 shows the resulting normalized current at different pressures in the chamber. As it can be noticed, the plume diverges with increasing pressure, as expected from the scattering off background gas atoms. Quantitatively, the plume divergence was calculated by finding the half-angle that contains 90% of the total integrated ion current. Here, the half-angle was found to increase from 15° to 45° across the investigated pressure range. Ongoing work aims to capture this effect into a higher fidelity quasi 2D model.

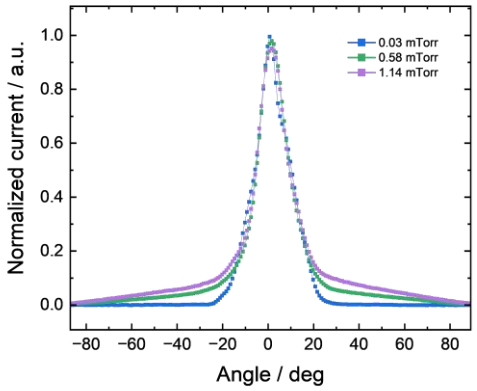

Fig. 8 Normalized ion current measured with a flat electrostatic probe with a guarding sleeve at different background pressures. Measurements were corrected for the background ion current.

Another possible issue is the pressure variation throughout the chamber. Complex flow patterns and pressure gradients could arise along the ion beam propagation path because of: (i) gas expansion from the ion source into the larger chamber; (ii) secondary gas influx from the top of the chamber; and (iii) turbopump located on the side of the chamber. To verify, we measured the spatial pressure profile within the chamber using a nude ion gauge (Kurt Lesker) installed on a movable rod. This allowed us to translate the ion gauge through the chamber to map the pressure at different distances from the ion source.

Figure 9 shows pressure values as measured with a nude ion gauge at varying distances from the ion source (green squares), plotted against the reference pressure obtained from a stationary gauge at the top of the chamber (blue line). While the data indeed indicates a presence of a pressure gradient, its magnitude falls largely within the ±15% measurement uncertainty of an ion gauge, and was therefore considered insufficient to explain the deviation of experimental CEX results from the theory.

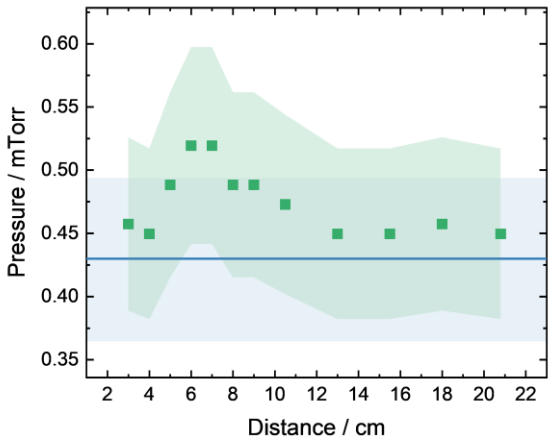

Fig. 9 Pressure values as measured with a movable nude ion gauge at different distances from the ion source (green). Blue line at 0.43 mTorr shows the pressure as measured with a stationary ion gauge at the top of the chamber. Filled areas represent a typical ion gauge accuracy of ±15%. Argon gas was supplied through the ion source at 4.6 sccm and directly into the main chamber at 65 sccm. Ion source was not operated during these measurements.

We note, however, that the ion source was inactive during these pressure measurements, and hence, this analysis leaves out possible pressure changes due to the ion beam propagation. For example, the ion beam travelling through the background gas could itself result in a pressure gradient, as reported by Kahn, Kaufman, et al., who observed a dynamic pressure rise in the direction of the ion beam [16]. Furthermore, fast ions reaching the chamber walls can neutralize and backscatter as neutrals. While the collector surface is protected from these particles with the ceramic holder, these neutrals could locally change the pressure.

Here, we roughly estimate the possible effect of neutrals originating from the ions backscattered from the chamber walls. When ions impact the chamber walls and neutralize, the resulting neutral density is bounded by two limiting cases: elastic backscattering and full thermalization. The maximum measured beam current in this work was 3 mA, as measured with a thermal probe at minimum background pressure of 0.03 mTorr and at the closest distance to the ion source (5 cm). For the argon ions at energy of 420 eV, this corresponds to the ion density, $n_i = \frac{I_i}{eAv_i} = 10^{15}$ cm^3, where I_i is the ion current, e is the elementary charge, A is the thermal probe collection area, and v_i is the ion velocity. Therefore, using the flux conservation, $n_\mathrm{i} v_\mathrm{i} = n_\mathrm{f} v_\mathrm{f}$, where n_i and v_i are initial density and velocity, and n_f and v_f are density and velocity after backscattering, the possible neutral densities lie between 10^{15}—10^{17} cm^3. In contrast, the background neutral density ranges between 10^{18}—10^{19} cm^{-3} for pressures between 0.03—1.14 mTorr. Consequently, even if all the ions created by the ion source reached the chamber walls, neutralized, and backscattered as neutrals, the ambient background gas density would still be at least an order of magnitude higher, confirming that wall-scattered neutrals are negligible.

Additional experiments are undergoing that deploy a Retarding Potential Analyzer aiming to resolve the ion energy distribution function at various background pressures. Preliminary results indicated a distinct population of low energy ions (< 10 eV) present in the beam, which fraction increases with distance and pressure. This trend is consistent with the generation of slow ions via charge-exchange collisions, as measured with the thermal flux probe. This also highlights the importance of accurately accounting for slow ions when characterizing the ion source plume, including CEX process. Details and the results of these measurements will be reported in an upcoming publication.

V. Conclusion

This study demonstrated the design, calibration, and deployment of a custom-made thermal flux probe for characterizing charge-exchange (CEX) process within an ion source plume. The experimental results confirmed that CEX ratios increase with both ambient pressure and distance from the source. Furthermore, as found from the

comparison between the experiment and the theory, the background pressure had a significant influence on the measurements, e.g., beam divergence and scattering, which are often left unaccounted in simple 1D models. Additionally, the creation of slow ions due to CEX was also found to affect the measurements. Finally, we reported encountered challenges with the thermal flux probe calibration and discussed their ongoing mitigation strategies.

Acknowledgments

We thank Dr. H. Sekine (currently on a sabbatical at PPPL) for help with the angular plume measurements and fruitful discussions, Timothy Bennett and Aleksandr Merzhevsky for technical support. This work was supported by the U.S. Department of Energy through Contract DE-AC02-09CH11466

References

[1] M. Stahl, T. Trottenberg, and H. Kersten, "A calorimetric probe for plasma diagnostics," *Review of Scientific Instruments*, vol. 81, no. 2, p. 023504, Feb. 2010, doi: 10.1063/1.3276707.

[2] J. A. Thornton, "Substrate heating in cylindrical magnetron sputtering sources," *Thin Solid Films*, vol. 54, no. 1, pp. 23–31, Oct. 1978, doi: 10.1016/0040-6090(78)90273-0.

[3] L. Rosenfeldt, L. Hansen, and H. Kersten, "The Use of Passive Thermal Probes for the Determination of Energy Fluxes in Atmospheric Pressure Plasmas," *IEEE Trans. Plasma Sci.*, vol. 49, no. 11, pp. 3325–3335, Nov. 2021, doi: 10.1109/tps.2021.3092752.

[4] A. Smirnov, Y. Raitses, and N. J. Fisch, "Plasma measurements in a 100 W cylindrical Hall thruster," *Journal of Applied Physics*, vol. 95, no. 5, pp. 2283–2292, Mar. 2004, doi: 10.1063/1.1642734.

[5] V. S. Smentkowski, "Trends in sputtering," *Progress in Surface Science*, vol. 64, no. 1, pp. 1–58, May 2000, doi: 10.1016/S0079-6816(99)00021-0.

[6] K. Oda, T. Kanie, A. Ichimiya, S. Ohtani, K. Ohya, and H. Tawara, "Secondary electron emission from a clean tantalum surface under keV rare gas neutral beam bombardment," *Surface Science*, vol. 262, no. 3, pp. 437–443, Feb. 1992, doi: 10.1016/0039-6028(92)90139-W.

[7] A. V. Phelps and Z. L. Petrovic, "Cold-cathode discharges and breakdown in argon: surface and gas phase production of secondary electrons," *Plasma Sources Sci. Technol.*, vol. 8, no. 3, pp. R21–R44, Aug. 1999, doi: 10.1088/0963-0252/8/3/201.

[8] C. E. Moore, *Atomic Energy Levels as Derived from the Analyses of Optical Spectra*, no. v. 1. in Atomic Energy Levels as Derived from the Analyses of Optical Spectra. U.S. Department of Commerce, National Bureau of Standards, 1949.

[9] M. A. Lieberman and A. J. Lichtenberg, *Principles of Plasma Discharges and Materials Processing: Lieberman/Plasma 2e*. Hoboken, NJ, USA: John Wiley & Sons, Inc., 2005. doi: 10.1002/0471724254.

[10] J. Cazaux, "e-Induced secondary electron emission yield of insulators and charging effects," *Nuclear Instruments and Methods in Physics Research Section B: Beam Interactions with Materials and Atoms*, vol. 244, no. 2, pp. 307–322, Mar. 2006, doi: 10.1016/j.nimb.2005.10.006.

[11] S. Gauter, "Calorimetric investigation on plasma and ion beam sources used for thin film deposition," Christian-Albrechts-Universität zu Kiel, Kiel, 2018. [Online]. Available: https://macau.uni-kiel.de/receive/diss_mods_00024040

[12] A. V. Phelps, "The application of scattering cross sections to ion flux models in discharge sheaths," *Journal of Applied Physics*, vol. 76, no. 2, pp. 747–753, Jul. 1994, doi: 10.1063/1.357820.

[13] S. Bromley, C. E. Sosolik, and J. P. Marler, "Symmetric charge exchange for intermediate velocity noble gas projectiles," *J. Phys. B: At. Mol. Opt. Phys.*, vol. 52, no. 21, p. 215203, Nov. 2019, doi: 10.1088/1361-6455/ab42d1.

[14] D. M. Goebel, I. Katz, and I. G. Mikellides, *Fundamentals of electric propulsion*. John Wiley & Sons, 2023.

[15] Y. Raitses, D. Staack, A. Dunaevsky, L. Dorf, and N.J. Fisch, "Preliminary Results of Plasma Flow Measurements in a 2 KW Segmented Hall Thruster," Princeton Plasma Physics Lab., NJ (US), US, PPPL-3796, Mar. 2003. doi: 10.2172/812923.

[16] J. R. Kahn, "Low-Energy End-Hall Ion Source Characterization at Millitorr Pressures," presented at the 48th Annual Technical Conference Proceedings, 2005.